Regular structures in 5CB liquid crystals under the joint action of ac and dc voltages

Luis E. Aguirre and Esteban Anoardo
LaRTE-FaMAF, Universidad Nacional de Córdoba and IFEG-CONICET Medina Allende y Haya de la Torre S/N, Ciudad Universitaria, X5016LAE Córdoba, Argentina

Nándor Éber and Ágnes Buka
Institute for Solid State Physics and Optics, Wigner Research Center for Physics, Hungarian Academy of Sciences, H-1525 Budapest, P. O. Box 49, Hungary
(Received 28 February 2012; published 19 April 2012)

A nematic liquid crystal with high, positive dielectric anisotropy (5CB) has been studied under the influence of the combined action of a dc and an ac electric field. Broad frequency, voltage, and cell thickness ranges were considered. Pattern morphologies were identified; the thresholds and critical wave numbers were measured and analyzed as a function of frequency, dc-to-ac voltage ratio, and thickness. The current-voltage characteristics were simultaneously detected.

DOI: 10.1103/PhysRevE.85.041703 PACS number(s): 61.30.Gd, 47.54.−r, 47.20.Lz, 64.70.M−

I. INTRODUCTION

Electric-field-induced patterns in nematic liquid crystals [1,2] can be of a different nature; either the free energy density drives the director field into a periodic distribution (equilibrium structure without fluid flow and without electric current) or an electrohydrodynamic destabilization occurs. In the latter case, the combined action of director distortion, fluid vortices, and formation of space charges is responsible for the pattern formation.

The space charge distribution may originate from different mechanisms. In the well-established theory of electroconvection (EC) in nematics the space charge formation is due to the conductivity anisotropy of the nematic medium (Carr-Helfrich mechanism) [3,4]. The coupling between the space charge and an electric field induces a convective flow, similarly to the temperature-gradient-driven Rayleigh-Bénard convection in isotropic fluids [5]. Examples of other mechanisms of charge separation include flexoelectric polarization [6] and the isotropic Felici instability [7,8]. The charge carriers in the system can originate [9] from the ionic impurities either contained by the liquid crystal or injected by the electrodes [7,10] or through electrochemical processes. The latter become especially important at low-frequency ac or dc fields.

EC instabilities are easily observed in nematic liquid crystals having a negative dielectric anisotropy ε_a and a positive conductivity anisotropy σ_a [3,4]; in the case of $\varepsilon_a > 0$ and $\sigma_a < 0$, patterns occur but less frequently [11]. In compounds with ε_a and σ_a both positive, however, the Carr-Helfrich mechanism [3] inhibits electroconvection. Despite that, electroconvective effects on applying an ac voltage have been observed in materials with $\varepsilon_a > 0$ and $\sigma_a > 0$ [12–14]. The frequency dependence of the threshold voltage indicated the existence of two patterns, fingerprint-like domains (found at low frequencies) and cross-shaped domains at high frequencies. Recent studies [15] using 5CB (4-pentyl-4′-cyanobiphenyl) confined in cells with planar or homeotropic alignments also pointed out the existence of electroconvective domains. In that work, another low-frequency morphology, a two-dimensional cellular pattern, was reported, too. It was found that the threshold voltages depend strongly on the frequency of the electric field, unlike the wave numbers that were almost insensitive to frequency changes (at least within the studied range).

Studies concerning pattern formation following the application of a dc voltage are less common. This is a consequence of potential pitfalls that may occur in electro-optical cells when subjected to electric excitation for extended periods (e.g., electrolytic effects, charge injection, and electrochemical degradation of the compound and of the electrodes).

The pattern formation in 5CB (and other homologs of cyanobiphenyls) under a pure dc voltage was studied by several authors. Nakagawa *et al.* [16] observed cellular structures in 25-μm cells with homeotropic alignment by applying only a dc voltage. The Felici mechanism involving charge injection was suggested to be the origin of the observed instabilities. The same mechanism was suggested to explain the honeycomb-like pattern, obtained in cells of 120 μm filled with 5CB by applying a dc voltage superposed to a laser beam [17]. Rout *et al.* found elongated domains developing from Maltese crosses in homeotropic cells of different thickness that define the wavelength [10,18].

A particular phenomenon related to the action of a dc voltage is the flexoelectric effect, which is a linear coupling between electric polarization and local director distortion in the liquid crystal [19,20]. The flexoelectric interaction may have a dipolar [19] or quadrupolar [21,22] character and becomes relevant especially for time-independent (dc) fields or for low-frequency alternating fields. Although the flexoelectric interaction is generally considered to be dominant near the electrode surface [23], flexoelectric domains were also claimed to exist in planar nematics within the volume [8,24,25].

Flexoelectric domains are, however, inhibited in compounds with large positive dielectric anisotropy like cyanobiphenyls. On applying a voltage, the initially planar nematic rather undergoes a Fréedericksz transition, yielding an almost homeotropic orientation in the bulk and large director gradients near the electrode surfaces (assuming a strong surface anchoring condition). The director gradients result in non-negligible flexoelectric polarization. While the dielectric interaction shows quadratic field dependence, the

flexoelectric polarization couples to the field in a linear way, like other surface polarization processes (which are related to polar adhesion of molecules to the substrates). This fact leads to completely different situations in the middle of the cell compared to spatial regions near the electrodes, particularly in thick cells.

Under certain conditions, the near-electrode layers may also become unstable. Such a polar surface instability has been reported in homeotropic 5CB subjected to pure dc excitation [26]. The pattern appeared at only one substrate and relocated to the other at changing the polarity of the field. Their formation was interpreted via a flexoelectric and, perhaps even more importantly, surface-polarization-driven mechanism. The static equilibrium structure provided by the instability evolves into a convective pattern at higher dc fields, which may "copy" the morphology of the underlying static structures, resulting in a similar optical appearance [27]. As the pattern occurs at the surface, the anchoring conditions play an important role in this phenomenon; e.g., weak anchoring favors the instability [26]. While patterns occurring at the pure ac or dc excitation have been studied in detail, combined ac + dc driving has not attracted attention. To our knowledge, mixed driving was tested only with flexodomains [25,28] but not for EC patterns.

In this paper we carry out a systematic study under the combined action of a dc and an ac electric field. In Sec. II we describe the experimental setup. In Sec. III the experimental results are presented. First, we describe the pattern morphologies at a fixed frequency, deducing a general phase diagram representing common features for a broad thickness range, and we then focus on the frequency dependence of pattern characteristics. We next discuss the formation of hexagonal patterns demonstrated on thick cells which allow an easier monitoring of the process due to longer director response times. Finally, we analyze the current-voltage characteristics and relate that to the pattern formation. We finish the paper with some concluding remarks.

II. EXPERIMENTAL SETUP

Measurements have been carried out on the nematic liquid crystal 5CB obtained from two different sources (Merck and Sigma-Aldrich). For the experiments, planar-aligned sandwich cells of different thicknesses, $d = 20$, 50, 127, 250 and 650 μm, were used. The cell gaps have been checked by optical interferometry and then filled with 5CB in the isotropic phase. The samples were placed into a microscope hot stage which held the temperature constant with a precision of ± 0.05 °C.

Applying a voltage V to the transparent electrodes produced an electric field through the cell. The behavior under the joint action of dc (V_{dc}) and ac (V_{ac}) voltages of frequency f were tested; V_{ac} will be reported as an rms value throughout the whole paper. The voltage was generated by an Agilent 33220A function generator which is capable of adding a dc offset to the ac voltage of sinusoidal waveform. Thus, $V = V_{dc} + V_{ac}\sqrt{2}\sin(2\pi f t)$. The generated voltage was applied to the cell either directly ($|V| < 10$ V) or through a homemade high-voltage amplifier (then $|V| < 200$ V).

The voltage-induced patterns have been observed using two independent setups. The thinner samples were investigated in a Leica DMRX polarizing microscope combined with a high-resolution digital camera from Optronics (1600 × 1200 pixels at 10 fps). For testing the other samples, a video microscopy setup, based on an Olympus BH2-SC microscope equipped with a RCA TC2014/X video camera, was used. Its video signals were digitized using an Encore ENLTV-FM PCI board, having a resolution of 720 × 576 at 30 fps. The sample was put between a crossed polarizer and analyzer, with the polarizer being parallel to the initial alignment of the nematic director in the cell (which was horizontal in all recorded pictures) and was illuminated by white light.

Measurements were done at different dc and ac voltages in order to explore the behavior in the V_{ac}-V_{dc} plane. The voltages were increased in steps, allowing the cell to rest for a period of ∼150 s after each voltage increment. If any change in the pattern was still detected at the end of this period, the waiting time was increased until no variations in the optical field were observed. In mapping the V_{ac}-V_{dc} plane, various strategies were tried, including measurements at fixed V_{ac}, at fixed V_{dc}, at a constant $R = V_{dc}/V_{ac}$ ratio, and at a constant $V_{ac} + V_{dc}$.

In addition to microscopic observations, the electric current flowing through the cell was also measured using an Agilent U1252A digital multimeter (resolution of ±10 nA) connected in series with the cell. The voltage was applied by a function generator Agilent 33220A through a homemade amplifier and measured with an Instec GDS-2062 oscilloscope. Measurements were carried out in voltage sweep mode, changing the voltage in steps of 0.5 V, with a waiting time of ∼120 s before current recordings in order to avoid the transients.

III. EXPERIMENTAL RESULTS

A. Pattern morphologies

Figure 1 shows a qualitative morphological phase diagram on the V_{ac}-V_{dc} plane, resuming the general results deduced from various cells at a fixed driving frequency of 20 Hz. Applying a voltage to the cell—independently of whether it is ac, dc, or mixed—the initial planar state becomes unstable, first,

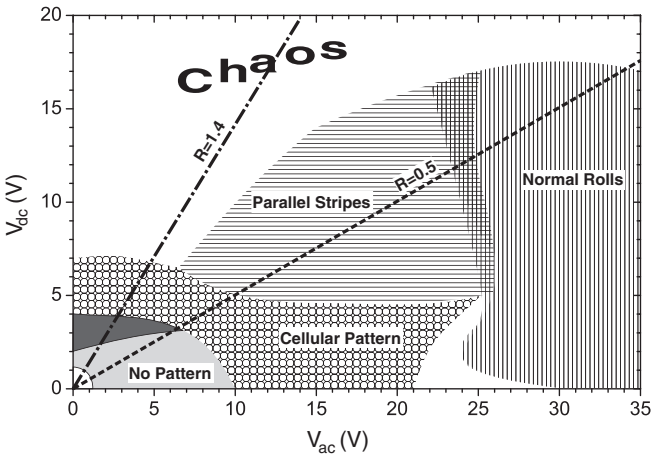

FIG. 1. Schematic qualitative morphological phase diagram of patterns at mixed voltage driving. The dashed and the dash-dotted lines represent fixed dc-to-ac voltage ratios of $R = 0.5$ and $R = 1.4$, respectively. The phase diagram corresponds to $f = 20$ Hz.

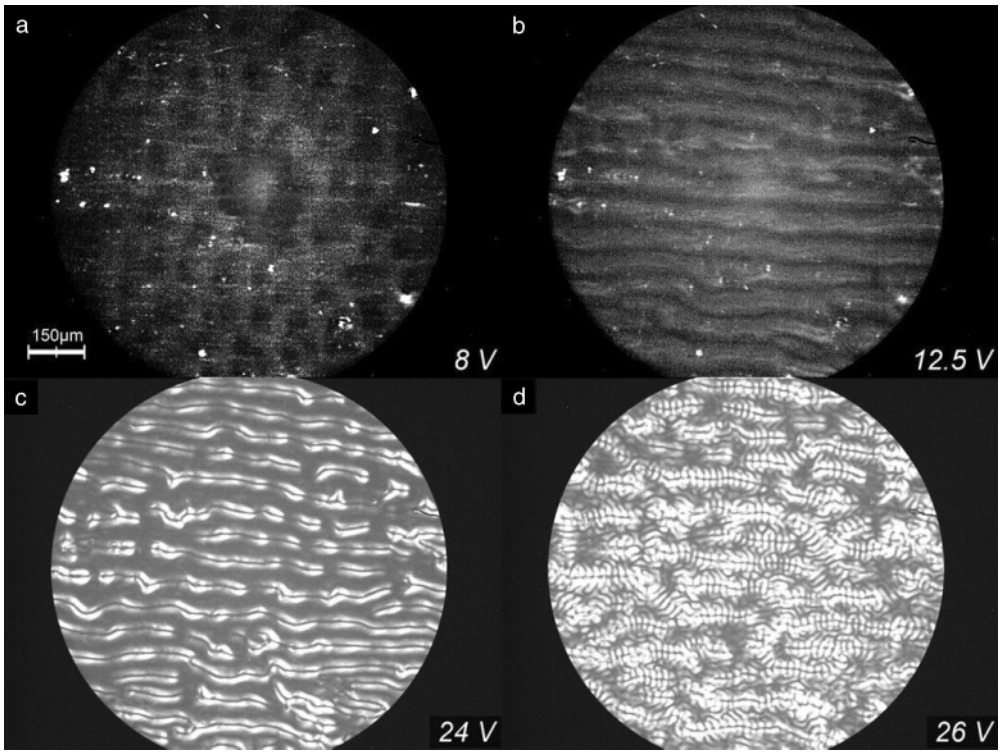

FIG. 2. Structures corresponding to different rms values of the ac voltage at a frequency of 20 Hz obtained in cells of 20 μm for a fixed $R = V_{dc}/V_{ac} = 0.5$ ratio. (a) Cellular pattern ($V_{ac} = 8.0$ V and $V_{dc} = 4.0$ V); (b) parallel stripes ($V_{ac} = 12.5$ V and $V_{dc} = 6.3$ V); (c) parallel stripes at higher voltages ($V_{ac} = 24.0$ V and $V_{dc} = 12.0$ V); and (d) herringbone pattern ($V_{ac} = 26.0$ V and $V_{dc} = 13.2$ V) corresponding to a superposition of parallel and normal rolls. The initial direction of the director is horizontal. Images (a) and (b) have undergone contrast-enhancing digital processing.

against the homogeneous splay Freedericksz transition [2,20] (see the thin circular line connecting the thresholds $V_{dc} \approx 1$ V with $V_{ac} \approx 1$ V). Patterns with various morphologies could be detected at much higher applied voltages; this implies a quasihomeotropic initial condition for their onset. Three characteristically different pattern morphologies—a *cellular pattern* (CP), *parallel stripes* (PS), and *normal rolls* (NR)—could be identified in various regions of the V_{ac}-V_{dc} plane. The cellular pattern is a two-dimensional network of convex domains, as it was defined earlier under pure ac driving [15]. Under certain conditions this structure orders into a hexagonal lattice. The existence region of CP extends to the pure ac or dc driving (horizontal or vertical axes in Fig. 1, respectively). This cellular structure appeared to be stationary; once it developed, the pattern remained stable for at least 24 h. Parallel stripes consist of a set of lines running parallel with the initial director alignment. To our knowledge, such a PS pattern [see Fig. 2(b)] has not yet been reported for 5CB or for any other nematics with the dielectric and conductivity anisotropies both positive. The existence region of PS does not extend to the pure ac or dc driving; thus, this structure emerges only under the combined action of V_{dc} and V_{ac}. Finally, the region representing normal rolls, i.e., rolls perpendicularly to the initial director alignment, persists from pure ac driving up to a relatively high added dc component. At very high voltages (independently of whether ac or dc) the system transforms into a rapidly fluctuating, irregular pattern denoted as *chaos* in Fig. 1.

We note that there is no sharp transition between the morphologies. The transition is either smooth (e.g., the cellular domains merge into elongated ones and, finally, into parallel stripes) or the two morphologies of neighboring regions coexist at around the region boundaries: see, e.g., the intermediate (square shaded) region where parallel and normal rolls are superposed, producing a *herringbone* pattern shown in Fig. 2(d). Furthermore, the transition from the CP to NR occurs via a nearly homogeneous state, to which the CP relaxes before the NR emerges (see the white region around $V_{ac} \sim 25$ V in Fig. 1). The threshold of the transition from the Freedericksz state to CP at low V_{ac} has a higher scattering for different cells (probably due to thickness dependence), as indicated by the gray region.

We demonstrate the above-described pattern morphologies and the transitions between them by varying the voltages at a fixed $R = V_{dc}/V_{ac}$ voltage ratio. As an example, in Fig. 2 we present an image gallery of various structures (clearly distinguishable by their morphological characteristics) obtained with increasing voltages at $R = 0.5$ (the dashed line in Fig. 1) for a driving frequency of $f = 20$ Hz in a thin ($d = 20$ μm) cell at (30.00 ± 0.05) °C. Please keep in mind that, though in the following figures we give only the rms values of the ac voltage, a dc offset corresponding to the fixed R is also applied simultaneously.

Figure 2(a) shows the emerged weak cellular structure. We note that the sum of the combined voltages $V_{ac} = 6.5$ V with

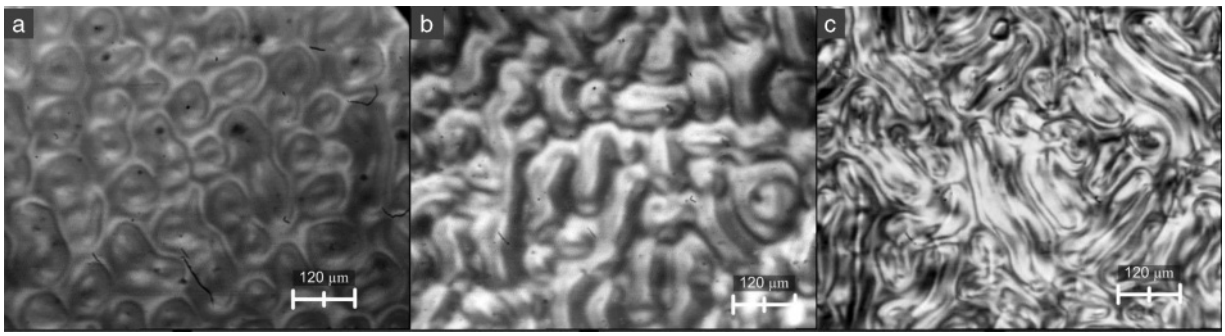

FIG. 3. Patterns observed in the $d = 127$ μm cell at $T = (25 \pm 1)\,^{\circ}$C. (a) Cellular pattern at $R = 0.94$ (3.2 V_{ac} at 50 Hz and 3 V_{dc}); (b) fusion of cellular structures into elongated domains on increase of the voltage at the same $R = 0.94$; (c) fluctuating electroconvection rolls at $R = 1.91$ (3.4 V_{ac} at 50 Hz and 6.5 V_{dc}).

$V_{dc} = 3.2$ V at the threshold for $R = 0.5$ nearly coincides with the purely ac-driven threshold ($V_{ac} \approx 10$ V, see Fig. 4(a) of Ref. [15]). Increasing the voltages the pattern develops into stripes running parallel to the initial direction of the director (at about $V_{ac} = 10.5$ V with $V_{dc} = 5.3$ V). Further increase of the voltages results in a substantial increase of the pattern contrast [Fig. 2(c)], until, at around $V_{ac} = 24.5$ V with $V_{dc} = 12.2$ V, a second roll pattern, normal to the parallel stripes (and the initial director), starts to emerge. The superposition of the two orthogonal patterns results in the appearance of the "herringbone" structure, shown in Fig. 2(d). At further increase of the voltages the normal rolls turn to be dominant over the parallel stripes and the pattern becomes strongly reminiscent of the roll pattern seen at pure ac driving [15]. We note that the patterns with relatively low-threshold voltages—the cellular pattern and the parallel stripes—are stationary in their appearance, in contrast to the normal rolls (herringbone), which are highly dynamic (the positions of rolls relocate in time). Raw (unprocessed) digital images of patterns shown in Figs. 2–4 and 7 and 8 are available as supplemental material [29]. The scenarios described above could be observed in the dc-to-ac voltage ratio range of $0.35 < R < 0.7$. As seen from Fig. 1, for smaller R the cellular structure and the high-voltage morphology (normal rolls) persist; however, the parallel stripes disappear. The region with $R > 0.7$ is important because it includes $|R| = \sqrt{2}$ (the dash-dotted line in Fig. 1), where the amplitude of the ac voltage equals the dc offset voltage. Therefore, for $|R| > \sqrt{2}$ (dc dominant), the polarity of the voltage applied to the cell (determined by V_{dc}) remains unchanged and only its magnitude varies with time, while for $|R| < \sqrt{2}$ (ac dominant), a polarity reversal of the voltage occurs twice within each driving period. This might be important (makes a qualitative difference) for flexoelectricity-driven effects.

The $R > 0.7$ part of the morphological phase diagram could partially be explored using thicker ($d = 127$ μm) cells. For $R = 0.94$ the stationary CP was observed [Fig. 3(a)] and then, on increasing the voltage much above the threshold, the cellular domains fused into elongated ones [Fig. 3(b)], which fluctuate and relocate dynamically. The studied voltage range, however, did not extend into the region where ordered parallel stripes [similar to those in Figs. 2(b) and 2(c)] might be expected.

For $R = 1.91$ (dc-dominant case), elongated, oblique, and disordered patterns of dynamic character rose up [shown in Fig. 3(c)] above the CP region, as a clear consequence of an electrohydrodynamic instability. A similar pattern was reported by Rout *et al.* for 8CB under dc excitation and interpreted in terms of the Felici mechanism [10].

A particular feature observed in certain conditions in the CP regime was the ordering of the randomly distributed domains into a hexagonally ordered lattice [30]. For thin cells, hexagons have been detected for pure ac driving, while for thick cells their most pronounced appearance was at around $R \sim 1.4$. The hexagons can be either regular or slightly irregular, as shown in Figs. 4(a) and 4(b), respectively. The hexagonal structures appeared to be of stationary nature, like the cellular pattern. Moreover, the cellular and the hexagonal patterns have the same wavelength and their onset process is similar.

Though the phase diagram of Fig. 1 provides a good summary of the pattern morphologies observed in several cells, it has to be noted that, despite of all their qualitative similarities, various cells had quantitative differences in the voltage values of the morphological transitions. On the one

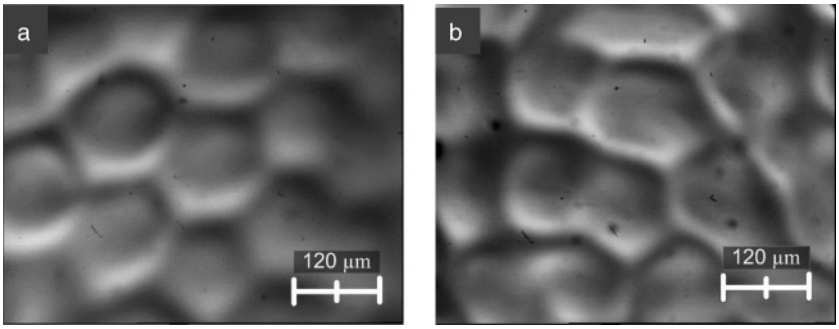

FIG. 4. (a) Regular hexagons obtained at $R \sim 1.4$ in $d = 127$ μm cells applying an ac voltage of 3 V. (b) Irregular hexagons, obtained under the same conditions, in a different cell position.

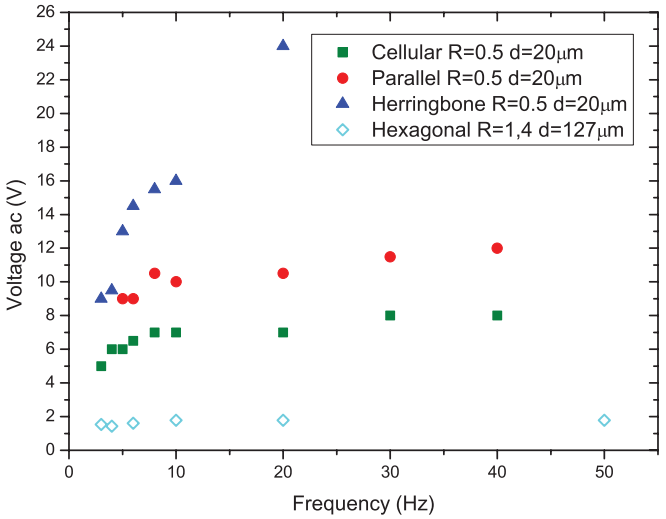

FIG. 5. (Color online) Frequency dependencies of the threshold voltage of various patterns.

hand, these differences may be attributed to the different cell thicknesses which, in certain cases, may also affect the appearance of a particular pattern morphology. On the other hand, the presence of nonzero dc voltages applied to the cell may play an important role. A dc voltage activates several additional effects (like Debye screening, charge injection, and electrochemical reactions) which have mostly been found negligible at the usual high-frequency ($f > 10$ Hz), pure ac driving. These phenomena are typically uncontrolled and can make the cell dependent on its voltage history, leading to larger uncertainties of regime boundaries. In addition, cells filled with 5CB from different sources also behaved slightly (quantitatively) differently; this may be associated to minor differences in some of their relevant material parameters, such as electric conductivity.

As all patterns appear much above the Freedericksz threshold voltage, the pattern formation occurs from a quasi-homeotropic state. Therefore, it is important to test, what happens if one starts from a homeotropically aligned sample ($d = 20$ μm) but otherwise the same conditions as discussed above. It is known from previous reports that the cellular pattern and normal rolls arise also in homeotropic cells at pure ac driving [15] and CP was seen as well at applying pure dc voltages [16]. Surprisingly, in contrast to the pure driving cases, no extended pattern was observed in the homeotropic sample at mixed voltage driving at $R = 0.5$. By increasing the voltages only localized point defects and irregular flow could be detected.

B. Frequency dependence

The morphological phase diagram depicted in Fig. 1 is qualitatively valid not only for a selected frequency but also for some frequency range. In order to illustrate this, similar measurements were carried out for different frequencies within the range of 3–40 Hz while keeping the ratio R fixed at ~0.5. Figure 5 shows the frequency dependence of the threshold voltages of the three characteristic pattern morphologies for $d = 20$ μm. It is evident that the cellular pattern and the parallel stripes were always observed at lower voltages compared to the threshold of the herringbone (normal roll) pattern. One has to note, however, that the parallel stripes could be detected only at frequencies greater than ~5 Hz; below this frequency only cellular and herringbone structures could be seen. The figure also indicates that the thresholds for the cellular and the parallel roll pattern types are only weakly affected by the frequency variation, at least within the analyzed range. In contrast to that, the threshold voltage of the herringbone structure is strongly frequency dependent, just as it has been reported recently [15] for the pure ac-induced roll patterns. In fact, for the last pattern morphology, we could register only the thresholds up to 20 Hz, since for higher frequencies the required dc voltage at $R \sim 0.5$ would degrade the cell.

For comparison we have included in the figure the threshold curve of the hexagonal pattern of a $d = 127$ μm cell, measured at $R \sim 1.4$. It is seen that this threshold ac voltage remains also almost frequency independent above 10 Hz. Note that this threshold voltage is lower than that of the cellular pattern in the thin cell, in correspondence with the higher R used in this case.

In addition to the threshold voltages the (critical) wave number of the pattern at onset is another important parameter characterizing the different pattern morphologies. Usually it is convenient to introduce a dimensionless critical wave number defined as $q = 2d/\lambda$, where d is the sample thickness and λ is the wavelength of the pattern (for the cellular pattern the diameter of a convex domain is taken as λ). λ could be obtained by averaging the wavelengths taken from several recorded images. Figure 6 shows the frequency dependence of the dimensionless critical wave numbers for a $d = 20$ μm cell (at $R \sim 0.5$), as well as for a $d = 127$ μm cell (at $R \sim 1.4$). It can be seen that q of the cellular, of the hexagonal and of the parallel stripe patterns remain almost constant with frequency. This result is similar to that previously obtained for the pure ac-induced patterns [15].

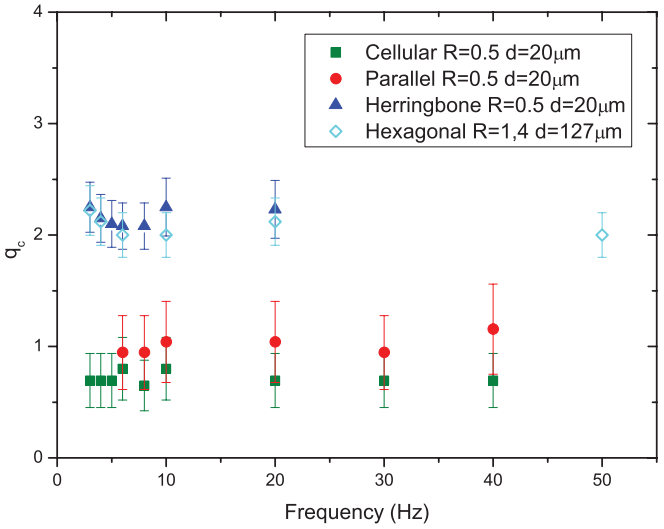

FIG. 6. (Color online) Frequency dependence of the critical wave numbers of various patterns, measured in a 20-μm-thick and in a 127-μm-thick cell.

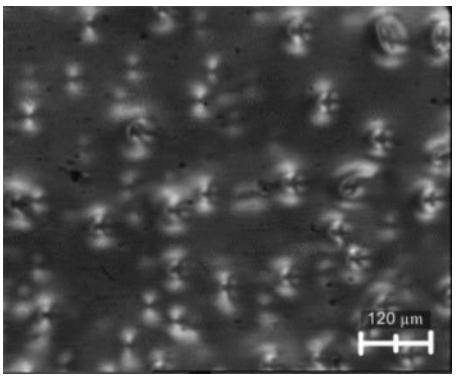

FIG. 7. Cell of 127 μm; initial point defects in the director reorientation observed after the Freedericksz transition at $R \sim 1.4$.

C. Formation of the hexagonal pattern

As mentioned above, in cells of 127 $\mu\text{m} \leqslant d \leqslant 250$ μm clear hexagonal structures were observed for mixed voltage driving at $R \sim 1.4$, while such structures did not appear in thick cells under the individual action of either ac or dc voltages (at least within the voltage ranges explored in this work). In cells of higher thickness the director reorientations are much slower than in thin cells, as the director relaxation time is $\propto d^2$. This fact allowed us to explore some details (the time evolution) of the pattern formation process leading to the formation of the hexagonal structures, which are given below. At the application of a combined dc and ac voltage with a fixed ratio of $R \sim 1.4$ to the cell, the sequence of events leading to the onset of hexagons starts with the splay Freedericksz transition. Increasing the applied voltage above the Freedericksz threshold, bright spots could be observed that evolve into Maltese crosses (Fig. 7).

By repeating the experiment in a relaxed cell (heated up and cooled down from the isotropic state), it could be verified that the positions at which the bright spots appear differ in each run. This suggests that these centers are not associated with permanent surface defects at the electrodes. These point singularities serve as seeds from where a circularly spreading instability starts to develop at a constant voltage. In a time lapse of about 3 min, the instability fronts originating from different seeds abut and start to interact with each other. The pattern evolves until, finally, a hexagonal structure is formed after a time lapse of about 17 min. Once the structure reaches a steady state, the positional order is maintained and, at most, only localized minor fluctuations can be observed. This stability of the structure has been checked by keeping the cell powered for about 24 h; during this time the pattern remained unchanged. This sequence of events occurred both for 127-μm- and 250-μm-thick cells.

The threshold voltages of the hexagonal pattern were $V_{ac} = 1.8$ V and $V_{ac} = 3.9$ V (at $R \sim 1.4$) for the 127-μm- and the 250-μm-thick cells, respectively. The average major diagonal of the hexagons was $\lambda \sim 130$ μm in $d = 127$ μm cells, while a value of $\lambda \sim 200$ μm was measured for the cell of 250-μm thickness. From these characteristic lengths one can calculate the critical dimensionless wave number as $q = 2d/\lambda$, yielding $q \sim 2$ and 2.3, respectively, for the two cells.

Figure 8(a) shows that bright spots, coinciding with the centers of the hexagons, can be observed, particularly when the focal plane of the microscope is adjusted nearby the electrodes. However, as soon as the focus moves inside the cell, the bright centers disappear [Fig. 8(b)], suggesting that the distortion of the original director at the points (crosses) occurs mostly near the surface of the cell.

The above observations point at the possibility of a surface instability preceding the CP (or hexagonal pattern) as well as at the important role of surface interactions. This latter is also supported by the fact that, under the same conditions, however, in cells without the PVA surface treatment, no structures were observed. The presence of patterns in ac + dc driven planar and their absence in homeotropic samples may call into question whether the polar instability reported by Monkade [26,27] could be the source of the bright spots. In planar 5CB the surface polarization should be much lower, but the flexoelectric polarization much larger than in the homeotropic sample. This offers the possibility that flexoelectric polarization may take over the role of surface polarization in the above instability mechanism. Nevertheless, other mechanisms leading to the formation of localized instabilities in the presence of a dc component, e.g., those due to charge injection [18], cannot yet be excluded.

D. Current measurements

Studies of the dc current flowing across the cells have provided additional information on the system. Figure 9 shows the current-voltage (I-V) characteristics for a thick ($d = 120$ μm) cell. The measured values are comparable to those obtained by Nakagawa *et al.* in ac-driven homeotropic cells [16], in the limit where the frequency of the electric field tends to zero. It is seen that the current response consists of two regimes: at low voltages the slope of the curve (conductivity) is very low (not detected with the given setup) and then it switches to a steep rise at around 3.5 V. This voltage is nearly

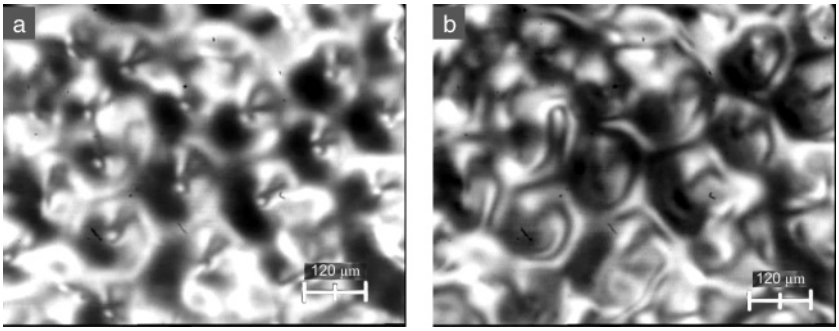

FIG. 8. (a) Hexagonal pattern at the surface electrode of the 127 μm cell; (b) same field but with the focal plane of the microscope shifted inward to the center of the cell.

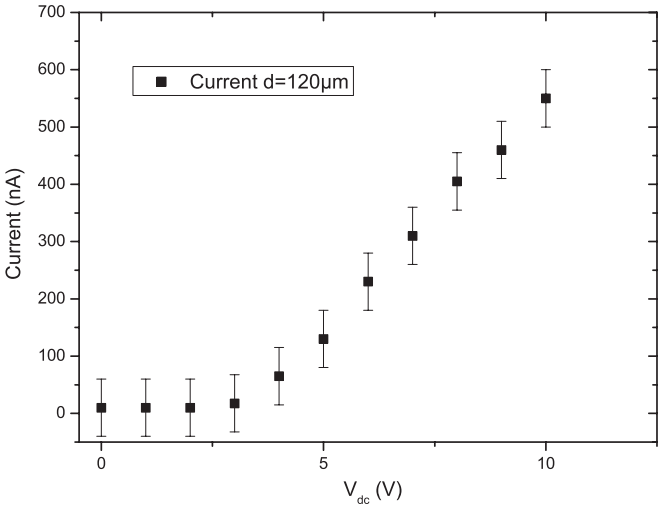

FIG. 9. Current-voltage characteristics of a $d = 120$ μm cell at dc driving.

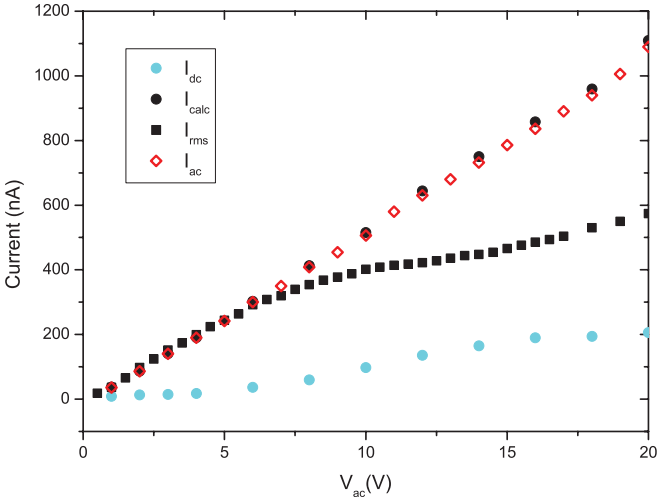

FIG. 10. (Color online) Current-voltage graphs for pure ac [$I_{ac}(V_{ac})$], pure dc [$I_{dc}(V_{dc})$], and mixed driving at $R = 0.5$ [$I_{rms}(V_{ac})$]. I_{calc} is the calculated rms current assuming simple superposition of ac and dc components.

coincident with the threshold value for the observed cellular pattern at pure dc driving. It suggests that the onset of the pattern might be associated with the substantial increase of the conductivity. We emphasize, however, that this latter effect cannot be the consequence of the director distortion, because a director tilt from the quasihomeotropic Freedericksz state would yield a decrease of the conductivity in a compound with positive σ_a; moreover, the induced conductivity change is expected to be negligible on this scale.

Note that the I-V characteristics in Fig. 9 qualitatively differ from those reported recently for a homeotropic 5CB [9]. The differences might originate, on the one hand, in the presence of a polyimide orienting layer in our planar samples which affects the charge transfer at the electrodes; on the other hand, the current in our sample was two orders of magnitude larger.

We have also tested how the I-V characteristics depend on the type of driving. In Fig. 10 the measured rms value of the current, I_{rms}, is plotted versus the ac voltage V_{ac} for the case of a mixed driving [$V(t) = RV_{ac} + \sqrt{2}V_{ac}\sin(2\pi f t)$] at $R = 0.5$. For reference we included the $I_{ac}(V_{ac})$ and $I_{dc}(RV_{ac})$ graphs measured independently at pure ac and dc driving, respectively. In case of a simple superposition of the ac and dc current components the rms value should be calculated as $I_{calc} = \sqrt{I_{ac}(V_{ac})^2 + I_{dc}(RV_{ac})^2}$. It is evident from Fig. 10 that the measured I_{rms} is substantially smaller than I_{calc} at higher voltages. Therefore, no simple superposition occurs at the mixed driving; the dc bias affects the ac conductivity as well. The deviation between I_{rms} and I_{calc} appears at $V_{ac} > 7$–8 V (corresponding to 3.5–4 V dc voltage), which is roughly the threshold voltage of the cellular pattern.

We have to emphasize again that the increasing I_{rms}-I_{calc} cannot be explained by the appearance of the cellular pattern. The director distortions involved are too small as follows from the low pattern contrast; therefore, the σ_a related decrease of the conductivity would yield a much smaller effect than that observed. This expectation is supported by electric current (Nusselt number) measurements in standard electroconvection [31]. Rather, we think that the current conduction mechanism suffers a considerable change at $V_{ac} \approx 7$–8 V, which initiates the onset of the pattern.

IV. DISCUSSION

Let us now compare the behavior and characteristics of the patterns observed at pure ac and at combined ac + dc driving. Figure 11 plots the threshold voltages versus the frequency for both types of driving (pure ac data were taken from Ref. [15]).

As we already mentioned [see Fig. 2(a)], the *cellular structure* observed in the thin cells at $R = 0.5$ (ac dominant) resembles those observed for the pure ac excitation in similar cells [15]: Both have a critical wave number within the range 0.5–0.7. A noticeable difference between the behavior at pure

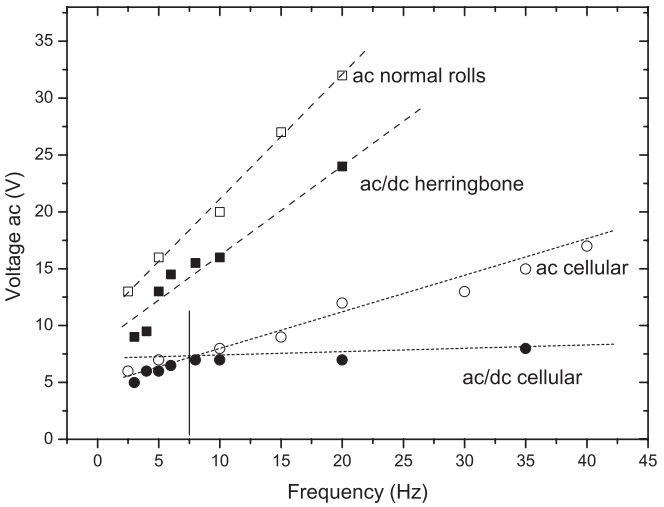

FIG. 11. Frequency dependence of the threshold voltages corresponding to the pure ac case (open symbols) and the combined ac/dc (solid symbols) excitation. Circles correspond to the cellular pattern while squares correspond to the herringbone (ac/dc) and normal rolls (ac) structures.

ac excitation and the mixed ac + dc case is seen, however, in the frequency dependence of the threshold voltage (compare Fig. 5 with Fig. 4(a) of Ref. [15]). While a steep linear frequency dependence was measured for the pure ac case, in the presence of a dc component two different regimes can be distinguished: At frequencies lower than about 7.5 Hz the dispersion is similar to that of the pure ac case, but the threshold becomes much less frequency dependent above that frequency (see Fig. 11). Moreover, from Fig. 11 one learns that the low-frequency values are similar in both cases. These facts clearly indicate that in the mixed ac + dc case the presence of the dc component affects substantially the instability mechanism at frequencies above 7.5 Hz.

The *parallel stripes* observed in thin cells [Fig. 2(b)] have similar critical wavelength as the cellular pattern and a similar frequency dependence of the threshold, although this pattern could not be observed at frequencies lower than 5 Hz. It is worth emphasizing that these parallel stripes appeared only in the presence of a dc component. Under the same conditions but using a homeotropic cell, no parallel stripes could be observed. This fact suggests that the driving mechanism for the parallel stripes could be of flexoelectric origin: In the planar configuration strong splay-bend deformations of the director field occur close to the electrodes. Note, however, that nonlinear effects of electric field distortion could also be considered, as they were found to lead to transient parallel stripes in 5CB during the splay Freedericksz transition (in the same geometry as here) [32].

Figure 11 also shows the measured frequency dependence of the threshold voltage for the pure ac-driven *normal rolls* as well as for the corresponding *herringbone* structure obtained at a combined ac + dc excitation at a fixed $R = 0.5$. It is immediately seen that the threshold voltages of both patterns grow linearly with f; however, the slope is considerably decreased by the dc offset in a similar manner as seen for the cellular pattern.

Summarizing, in this paper we presented a general experimental study and characterization of the pattern properties detected in the nematic liquid crystal 5CB subjected to the combined action of dc and ac electric fields. An important finding is a new kind of pattern (parallel stripes) observed under the joint action of both excitations and in the planar configuration only. This indicates a possible role of flexoelectricity and/or that of nonlinear effects of electric field distortion. A cellular pattern already observed for the pure excitation cases were also studied at different electro-optical cell gaps. For a given range of dc-to-ac voltage ratio, the cellular pattern evolved into a hexagonal structure. Using thick cells it was possible to follow the time evolution of this pattern onset. In contrast to the pure ac case, the frequency dependence of the threshold voltages in the presence of a dc offset turned out to be much weaker, even for structures having a similar morphology (independently of the cell gap). Current measurements also revealed that the presence of the dc component may cause a substantial modification of the ac conductivity.

Although we have enough evidence that the dc offset strongly affects the instability properties in the cell, still more information is needed to disentangle the possible mechanisms (or combination of them) that may drive the different pattern formations. Further experimental studies are in progress in order to find out more information on the director distribution of the observed patterns by means of confocal microscopy.

ACKNOWLEDGMENT

This work was partially supported by the bilateral Argentinian-Hungarian cooperation project HU/08/01 (Ministerio de Ciencia, Tecnología e Innovación Productiva) and OMFB-01290/2009 (Hungarian National Innovation Office). We thank T. Tóth-Katona for fruitful discussions, the group of Physics of the Atmosphere (FaMAF-Universidad Nacional de Córdoba) for access to infrastructure, and Alaide Mammana (Associação Brasileira de Informática) and Victor Mammana (Centro de Tecnologia da Informação Renato Archer) for technological advice in the construction of electro-optical cells. Financial help from the Hungarian Research Fund under Contract No. OTKA-K 81250, CONICET-Argentina, and Ministerio de Ciencia y Tecnología de la Provincia de Córdoba are gratefully acknowledged. L.A. was supported by a CONICET fellowship.

[1] A. Buka and L. Kramer, *Pattern Formation in Liquid Crystals* (Springer-Verlag, New York, 1996).
[2] L. M. Blinov and V. G. Chigrinov, *Electrooptic Effects in Liquid Crystal Materials* (Springer, New York, 1994).
[3] W. Helfrich, J. Chem. Phys. **51**, 4092 (1969).
[4] L. Kramer and W. Pesch, in *Pattern Formation in Liquid Crystals*, edited by A. Buka and L. Kramer (Springer-Verlag, New York, 1996), p. 221.
[5] M. C. Cross and P. C. Hohenberg, Rev. Mod. Phys. **65**, 851 (1993).
[6] A. Krekhov, W. Pesch, N. Éber, T. Tóth-Katona, and A. Buka, Phys. Rev. E **77**, 021705 (2008).
[7] N. Felici, Rev. Gen. Electr. **78**, 17 (1969).
[8] S. A. Pikin, *Structural Transformations in Liquid Crystals* (Gordon and Breach, New York, 1991).
[9] P. P. Korniychuk, A. M. Gabovich, K. Singer, A. I. Voitenko, and Y. A. Reznikov, Liq. Cryst. **37**, 1171 (2010).
[10] D. K. Rout and R. N. P. Choudhary, J. Phys. D **22**, 289 (1989).
[11] A. Buka, N. Éber, W. Pesch, and L. Kramer, in *Self-Assembly, Pattern Formation and Growth Phenomena in Nano-Systems*, NATO Science Series II, Mathematica, Physics and Chemistry, edited by A. A. Golovin and A. A. Nepomnyashchy (Springer, Dordrecht, 2006), pp. 55–82.
[12] R. A. Kashnow and H. S. Cole, Mol. Cryst. Liq. Cryst. **23**, 329 (1973).
[13] M. I. Barnik, Sov. Phys. JETP **45**, 396 (1977).
[14] D. K. Rout and R. N. P. Choudhary, Liq. Cryst. **4**, 393 (1989).
[15] P. Kumar, J. Heuer, T. Tóth-Katona, N. Éber, and A. Buka, Phys. Rev. E **81**, 020702 (2010).

[16] M. Nakagawa and T. Akahane, J. Phys. Soc. Jpn. **52**, 3773 (1983).
[17] L. Song and W.-K. Lee, Opt. Commun. **259**, 293 (2006).
[18] D. K. Rout and R. N. P. Choudhary, Mol. Cryst. Liq. Cryst. **154**, 241 (1988).
[19] R. B. Meyer, Phys. Rev. Lett. **22**, 918 (1969).
[20] J. Prost and P. de Gennes, *The Physics of Liquid Crystals* (Clarendon Press, Oxford, 1993).
[21] J. Prost and J. Marcerou, J. Phys. (France) **38**, 315 (1977).
[22] H. P. Hinov, I. Bivas, M. D. Mitov, K. Shoumarov, and Y. Marinov, Liq. Cryst. **30**, 1293 (2003).
[23] W. Helfrich, Appl. Phys. Lett. **24**, 451 (1974).
[24] Y. P. Bobylev and S. Pikin, Zh. Eksp. Teor. Fiz. **72**, 369 (1977).
[25] Y. Marinov, H. P. Hinov, and A. G. Petrov, J. Optoelectr. Adv. Mat. **7**, 277 (2005).
[26] M. Monkade, P. Martinot-Lagarde, and G. Durand, Europhys. Lett. **2**, 299 (1986).
[27] O. D. Lavrentovich, V. G. Nazarenko, V. V. Sergan, and G. Durand, Phys. Rev. A **45**, R6969 (1992).
[28] Y. Marinov, A. G. Petrov, and H. P. Hinov, Mol. Cryst. Liq. Cryst. **449**, 33 (2006).
[29] See Supplemental Material at http://link.aps.org/supplemental/10.1103/PhysRevE.85.041703 for raw (unprocessed) digital images of patterns shown in Figs. 2–4 and 7 and 8.
[30] L. Aguirre, A. Mammana, and E. Anoardo, in *SID Conference Record of the International Display Research Conference*, edited by Victor P. Mammana (Society for International Development, São Paulo, Brazil, 2010), pp. 83–89.
[31] J.T. Gleeson, N. Gheorghiu, and E. Plaut, Eur. Phys. J. B **26**, 515 (2002).
[32] A. Buka and L. Kramer, Phys. Rev. A **45**, 5624 (1992).